

# The impact of long-term changes in ocean waves and storm surge on coastal shoreline change: A case study of Bass Strait and south-east Australia

Mandana Ghanavati<sup>1</sup>, Ian R. Young\*<sup>1</sup>, Ebru Kirezci<sup>1</sup>, Jin Liu<sup>1</sup>

<sup>1</sup>Department of Infrastructure Engineering, University of Melbourne, Melbourne, VIC 3010, Australia.

\* Corresponding author: ian.young@unimelb.edu.au

## Abstract

Numerous studies have demonstrated that significant global changes in wave and storm surge conditions have occurred over recent decades and are expected to continue out to at least 2100. This raises the question as to whether the observed and projected changes in waves and storm surges, will impact coastlines in the future? Previous global-scale analyses of these issues have been inconclusive. This study investigates the south-east coast of Australia over a period of 26 years (1988-2013). Over this period, this area has experienced some of the largest changes in wave climate of any coastal region, globally. The analysis uses high-resolution hindcast data of waves and storm surge, together with satellite observations of shoreline change. All datasets have been previously extensively validated against in situ measurements. The data are analysed to determine trends in each of these quantities over this period. The coastline is partitioned into regions and spatial consistency between trends in each of the quantities investigated. The results show that beaches along this region appear to have responded to the increases in wave energy flux and changes in wave direction. This has enhanced non-equilibrium longshore drift. Long sections of the coastline show small but measurable recession before sediment transported along the coast is intercepted by prominent headlands. The recession is largest where there are strong trends of increasing wave energy flux and/or changes in wave direction, with recession rates of up to 1m/year. Although a regional study, this finding has global implications for shoreline stability in a changing climate.

## 1. Introduction

Sandy coastlines are dynamic systems, responding to changes in waves, storm surge, sea level, available coastal sediment supply and human activities (e.g. coastal structures, beach nourishment) (Komar, 1998; Masselink, et al., 2016). These changes occur on a variety of spatial and temporal scales. Spatially, changes in beach alignment and the presence of coastal shoreline features (headlands and bays) impact both the wave climate for individual beaches and the characteristics of longshore drift. At temporal scales of days, beach erosion results from individual storms (Komar, 1998; Harley, et al., 2017; Masselink, et al., 2016). At time scales of 2 to 10 years, changes in storminess associated with climate indices (e.g. El Niño) (Ranasinghe, et al., 2004; Harley, et al., 2011; Barnard, et al., 2015; Vos, et al., 2023) can result in sustained impacts on beach systems. Longer term changes in mean sea level as a result of climate change are also predicted to result in coastal recession (Hinkel, et al., 2013; Ranasinghe, 2016; Vousedoukas, et al., 2020; Ranasinghe, et al., 2021; Vitousek, et al., 2023). It should be noted that throughout this paper

39 we refer to shorter-term changes in beach location due to storms or a series of storms as erosion  
40 or accretion. Longer-term changes such as those due to climate change are referred to as recession  
41 or progradation.

42 Waves and storm surges are generated by environmental variables (wind and sea level pressure  
43 gradient). It has been shown that these environmental variables are impacted by climate change  
44 and hence long-term historical changes (trends) in waves (Wang & Swail, 2001; Wang, et al.,  
45 2009; Hemer, 2010; Young, et al., 2011; Aydoğan & Ayat, 2018; Zheng & Li, 2017; Young &  
46 Ribal, 2019; Takbash & Young, 2020; Reguero, et al., 2019; Cao, et al., 2021) (Young & Ribal,  
47 2022; Liu, et al., 2022; Morim, et al., 2022; Erikson, et al., 2022) and storm surges (Paprotny,  
48 2014; Androulidakis, et al., 2015; Cid, et al., 2016; Muis, et al., 2016; Kim, et al., 2017; Feng, et  
49 al., 2018; Ghanavati, et al., 2023) have been observed. A number of studies have also projected  
50 continued global increases (positive trends) in wave height over the 21<sup>st</sup> century, particularly in  
51 the Southern Hemisphere, under plausible climate change scenarios (Hemer, et al., 2013; Meucci,  
52 et al., 2020; Hochet, et al., 2021; Liu, et al., 2022; Meucci, et al., 2023; Morim, et al., 2023; Liu,  
53 et al., 2023).

54 If sandy coasts are impacted by changes in wave and storm surge conditions, the potential for  
55 continued increases in the values of these variables in **the future raises** the question as to what  
56 impact this may have on sandy coastlines and associated communities. As a means of determining  
57 potential future impacts, the obvious precursor is to assess the impacts that historical changes in  
58 long-term wave and storm surge conditions have had on coastlines. **In the first study of its type,**  
59 Ghanavati, et al. (2023) investigated this issue at global scale by using long-term modelled wave  
60 and storm surge data together with satellite observations of beach recession/progradation over the  
61 last 30 years. They found that, noting the relatively small trends in wave and storm surge conditions  
62 over this period, the accuracy of the available data, and other **unrelated** impacts on shoreline  
63 response (e.g. availability of sediment, human impacts), no clear relationship was evident.

64 **In order to address the limitation of the Ghanavati, et al (2023) work, the present study examines,**  
65 **in much finer detail,** the south-east coastline of Australia. This is an area where long-term trends  
66 in wave conditions are some of the largest in the world, responding to changes in wave climate in  
67 the Southern Ocean (Liu, et al., 2022). **Therefore, if there is a causal link between changes in long-**  
68 **term wave and storm surge climate and shoreline response, one would expect clear signs in this**  
69 **region.** As a regional area is considered, it is possible to use higher resolution data (both model  
70 and satellite) removing uncertainties in the global-scale Ghanavati, et al (2023) study. **In addition,**  
71 **the regional-scale study enables an analysis of the role beach compartments play in defining**  
72 **sediment transport. As such, one can investigate changes in longshore drift due to changes in wave**  
73 **climate and the characteristic signature of such non-equilibrium transport with eroding beaches**  
74 **and deposition of sediment behind peninsulas.**

75 **Although the present study is regional, the area being studied is a proxy for the potential impacts**  
76 **one may see in other regions of the world as changes in wave and storm surge climate are projected**

77 to continue to change in the future. Hence, the findings of the study have global implications for  
78 shoreline response in the future. The study is unique in that it has been possible to combine high  
79 resolution datasets for waves, storm surge and shoreline response and addresses a previously  
80 unexplored area of shoreline response in a changing climate.

81 The structure of the paper is as follows. Section 2 outlines the study area, data sets and analysis  
82 techniques used in the study. Results are given in Section 3, including the observed relationships  
83 between changes in wave and storm surge quantities and beach recession/progradation. Discussion  
84 and conclusions are provided in Section 4.

85

## 86 **2. Methodology**

87

### 88 **2.1 Study Area**

89 The study region is shown in Figures 1 and 2, and covers an area of 137E°–155°E, 35S°–45°S.  
90 Three Australian coastal states span this domain, Victoria, southern New South Wales and the  
91 island of Tasmania in the south of the domain. The south-eastern coast of the mainland of Australia  
92 (Victoria), the coastal area of the study, is separated from Tasmania by the relatively shallow Bass  
93 Strait. The area is exposed to a particularly complex wave climate (Liu, et al., 2022). To the west,  
94 the coast is exposed to the Southern Ocean and hence experiences a very energetic wave climate  
95 with recorded significant wave height as high as 10m (Meucci, et al., 2023). The wave climate of  
96 this region is dominated by south-westerly Southern Ocean swell. Central regions of the study  
97 domain are protected by the island of Tasmania and have a mixed wave climate with swell from  
98 both the south-west and south-east and locally generated wind sea. To the east, the wave climate  
99 is more heavily dependent on the local wind-sea but with south-easterly swell still playing a role  
100 (Liu, et al., 2022).

101

102 Both observational data from satellite altimeters (Young, et al., 2011; Young & Ribal, 2019;  
103 Timmermans, et al., 2020) and model hindcasts (and reanalyzes) (Cao, et al., 2021; Young &  
104 Ribal, 2022) show that over the last 35 years, there has been a small global increase in mean  
105 significant wave height. This increase is largest in the Southern Ocean (approximately 3mm/year  
106 or an increase of 3% over the last 30 years), which results in impacts across the Indian, South  
107 Pacific and South Atlantic Oceans due to radiating swell. Therefore, the study area is a location  
108 where relatively large changes in significant wave height have occurred over the period.

109

### 110 **2.2 Datasets**

111 This study uses regional datasets for each of wave, storm surge, and coastal change from which  
112 the historical trend magnitudes of the various quantities were calculated. The datasets under  
113 consideration cover different periods of time, and thus, to ensure consistency across analyses, a

114 common time period from 1988 to 2013 was selected. A description of each dataset used in the  
115 study is provided below.

116

117 *Liu et al. (2022) regional wave hindcast* is a high-resolution regional wave hindcast dataset based  
118 on a WAVEWATCH III model with an ST6 physics package (Liu, et al., 2021). The regional  
119 model covers the domain shown in Figure 2 using an unstructured grid with a coastal resolution  
120 as small as 500m and a coarser deep water resolution as large as 10km. The regional model is  
121 nested within a global model using the same ST6 physics (Liu, et al., 2021). Both the regional and  
122 global models are forced with ERA5 winds (Hersbach, et al., 2020). The regional wave model  
123 dataset has been extensively validated (Liu, et al., 2022; Liu, et al., 2023) against both a network  
124 of coastal buoys and satellite altimeter data. Wave data were available from the hindcast with a  
125 temporal resolution of 1 hour. The period of the hindcast was from 1981 to 2020. The dataset's  
126 high resolution is particularly important for studying coastal regions, where wave conditions can  
127 vary significantly over short distances. Additionally, the long period of coverage allows us to  
128 identify and analyze trends in the wave climate over several decades, providing insight into the  
129 possible effects of historical climate change on the region.

130

131 *Colberg, et al. (2018) Australian water level hindcast* is a dataset of sea level simulations for the  
132 Australian coastline. The dataset was generated using the Regional Ocean Modelling System  
133 (ROMS) (Shchepetkin & McWilliams, 2005), which was run in a depth-integrated form on a 5 km  
134 resolution grid for the Australian region. Tidal currents and heights at open boundaries were  
135 specified from the TPXO7.2 global model (Egbert & Erofeeva, 2002). TPXO7.2 best fits (in a  
136 least squares sense) the Laplace tidal equations and along track averaged data from  
137 TOPEX/Poseidon and Jason altimetry data. The ROMS model was run for the period 1981-2013  
138 and was forced with NCEP Climate Forecast System Reanalysis (CFSR) (Saha, et al., 2010) wind  
139 and surface pressure data. The model has been validated at 14 tide gauge locations around the  
140 Australian coastline (Colberg, et al., 2018). Again, the output was available on an hourly basis.

141 *Bishop-Taylor et al., (2021) Geoscience Australia beach dataset* is a high-resolution regional  
142 dataset of shoreline change rate for the coast of Australia. The dataset utilizes a combination of  
143 satellite visual data and tidal modelling to map shoreline change, with an along-coast resolution of  
144 30m for non-rocky (sandy or muddy) areas. The dataset provides annual values of the shoreline  
145 position over the period 1988 to 2019. The dataset has been extensively validated using in-situ  
146 measurements, comprising 330 validation transects, each spanning over 10 years of coastal  
147 monitoring data. The Mean Absolute Error (MAE) in the trend across these validation points was  
148 0.35 m/year (Bishop-Taylor, et al., 2021).

### 149 **2.3 Trend calculation**

150 Each of the datasets (waves, storm surge, shoreline location) are defined at different resolution and  
151 in different manners (structured and unstructured grids, specific shoreline positions), therefore  
152 none of these quantities are co-located. As shown by Ghanavati, et al., (2023) and subsequently

153 confirmed in Figures 3, 4 and 5, trends in both wave height and storm surge quantities generally  
154 vary smoothly along extended coastal regions (100s of kilometres). Shoreline  
155 recession/progradation rate can, however, vary rapidly in magnitude and sign over relatively short  
156 spatial scales (10s of kilometres) (Luijendijk, et al., 2018; Ghanavati, et al., 2023). That is, one  
157 beach can be receding whilst the next is prograding. As such, simple scatter plots of rates of change  
158 of wave and storm surge quantities verses recession/pogradation rates are not meaningful. Rather,  
159 one needs to consider relationships over spatial regions of the coastline. To achieve such an  
160 analysis, we divide the study domain in Figure 1 into six regions, each spanning  $2^\circ$  in longitude –  
161 (a)  $138^\circ\text{E}$ - $140^\circ\text{E}$ , (b)  $140^\circ\text{E}$ - $142^\circ\text{E}$ , (c)  $142^\circ\text{E}$ - $144^\circ\text{E}$ , (d)  $144^\circ\text{E}$ - $146^\circ\text{E}$ , (e)  $146^\circ\text{E}$ - $148^\circ\text{E}$  and (f)  
162  $148^\circ\text{E}$ - $150^\circ\text{E}$  from west to east. These regions span the differing wave climates of the study  
163 domain (see Figure 2 and subsequent discussion). For analysis purposes, we present data as  
164 follows. Wave quantities are presented both as colour shaded plots, and at shoreline locations  
165 corresponding to ocean points defined by the unstructured WAVEWATCH III computational grid.  
166 Storm surge quantities are shown at the locations corresponding to the ocean points nearest the  
167 land/sea transition of the ROMS 5km computational grid. Coastal change points are as defined at  
168 coastal locations in the Bishop-Taylor et al., (2021) dataset, which has an along-cost resolution of  
169 30m.

170 Each of the three datasets used in the study covers a different period of time: wave hindcast - 1981  
171 to 2020, storm surge data - 1981 to 2013, and shoreline change data - 1988 to 2019. To ensure a  
172 consistent evaluation of the trends and variability in the oceanic parameters, a common analysis  
173 period of 1988 to 2013 was selected for the study.

174 For each of the datasets, a range of quantities to be investigated were calculated. These include:  
175 waves – mean significant wave height ( $H_s$ ), 95<sup>th</sup> percentile significant wave height ( $H_s^{95}$ ), mean  
176 wave energy flux ( $C_g E$ ), mean wave period ( $T_m$ ) and mean wave direction ( $\theta_m$ ), where  $C_g$  is the  
177 group velocity of waves and  $E = H_s^2 / 16$  is the wave energy. The hourly data from the regional  
178 wave model was used to calculate annual values of each of these quantities.

179 As noted above, various datasets have different temporal and spatial resolutions and hence slightly  
180 different approaches were used to evaluate the variability and extremes of oceanic parameters. The  
181 wave and surge time series were collected at a temporal resolution of 1 hour, while the shoreline  
182 dataset provided annual shoreline change with reference to the shoreline location in 2019.  
183 Therefore, annual mean values of wave parameters including significant wave height, wave energy  
184 flux, wave direction and wave period were calculated. Furthermore, the extremes were determined  
185 by calculating annual higher percentiles (95th, 98th, and 99th) for significant wave height and  
186 surge level. These metrics provide a consistent basis for evaluating the variability and extremes of  
187 the oceanic parameters across different datasets. As the various percentile thresholds gave similar  
188 results, extreme events were determined as occasions on which the time series exceeded the 95<sup>th</sup>  
189 percentile but with such events separated by a minimum of 48 hours. The number of such events

190 in each year were defined as  $N_{H_s^{95}}$ . In a similar fashion, storm surges were defined as occasions  
 191 when the water surface elevation,  $\eta$ , exceeded the 95<sup>th</sup> percentile ( $\eta^{95}$ ) and the number of such  
 192 events was defined as  $N_{\eta^{95}}$ . Again, annual values of these quantities were determined. The annual  
 193 values of shoreline position from the Bishop-Taylor et al. (2021) data were defined in a similar  
 194 manner and represented as  $C_{GA}$ .

195 The annual values of each quantity were then used to determine linear trends over the period 1988-  
 196 2013. Both linear regression and the non-parametric Tiel-Sen estimator (Sen, 1968) were used for  
 197 this purpose. As the resulting values were very similar, the Sen slope estimates are used in the  
 198 subsequent analysis. The resulting trend values are represented as:  $\Delta H_s$ ,  $\Delta H_s^{95}$ ,  $\Delta C_g E$ ,  $\Delta \theta_m$ ,  
 199  $\Delta N_{H_s^{95}}$ ;  $\Delta \eta^{95}$ ,  $\Delta N_{\eta^{95}}$ ;  $\Delta C_{GA}$ .

200

### 201 3. Results

#### 202 3.1 Wave climate

203 Figure 2 shows the mean wave climate of the study area and how it has changed over the period  
 204 1988 to 2013 as indicated by the Liu, et al. (2022) hindcast. Figures 2a and 2b show the mean  
 205 significant wave height  $\bar{H}_s$  and wave energy flux,  $\overline{C_g E} = \rho g^2 H_s^2 T_m / (64\pi)$ , respectively. As  
 206 noted above, the significant wave height and wave energy flux vary significantly across the study  
 207 area. In the west, the coastline is exposed to energetic Southern Ocean swell with mean  $H_s$  of  
 208 approximately 3m. In the eastern regions of the study area, where there is protection provided by  
 209 the island of Tasmania, mean  $H_s$  decreases significantly to less than 1.5m, a decrease by a factor  
 210 of approximately 2. The wave energy flux shows an even more significant change, with mean  
 211 values varying from approximately 60kW/m in the west to 15kW/m in the east, a factor of 4. The  
 212 substantial reduction in wave energy flux is attributed to the protection provided by the island of  
 213 Tasmania, which leads to a decrease in both  $H_s$  and  $T_m$ . As shown by Liu, et al. (2022), the  
 214 mean/peak wave direction also changes significantly across the domain. In the west, the dominant  
 215 wave direction is defined by energetic south-westerly swell. In the east, the protection provided by  
 216 the island of Tasmania means that swell entering the area is predominately from the south-east.

217 The changes in wave climate over the study period are also significant across this region. As noted  
 218 above, a range of studies have shown that the Southern Ocean wave climate has increased over the  
 219 past 35 years (Young, et al., 2011; Young & Ribal, 2019; Cao, et al., 2021; Young & Ribal, 2022).  
 220 Swell from the Southern Ocean dominates the western areas of the study region and hence there  
 221 have been significant changes in the wave climate, as shown by Figures 2c-h. In the west,  $H_s$  has  
 222 increased by approximately 5% (Figure 2c) over the study period and  $C_g E$  by approximately 14%  
 223 (Figure 2d). In contrast, in the east, where the wave climate is not as exposed to Southern Ocean  
 224 swell, these values decrease to approximately zero (no change). Figures 2e and f clearly show that

225 the positive trends in  $H_s$  are due to changes in both swell and local wind-waves. Figure 2g also  
226 shows that there have been only small changes in  $T_m$  across the domain.

227 The most dramatic changes in wave climate concern the mean wave direction,  $\theta_m$ . Over the  
228 western regions of the study domain, there has been a small counter-clockwise rotation of the mean  
229 wave direction (less than  $1.5^\circ$ ). This is a result of the gradual southward movement of Southern  
230 Ocean low pressure systems over recent decades (Morim, et al., 2022). This small change in deep  
231 water wave direction, significantly impacts the shadow region in the lee of Tasmania and hence  
232 the wave direction, resulting in much larger counter-clockwise rotations of approximately  $5^\circ$   
233 (Figure 2h). These values reduce towards the coast of mainland Australia (eastern area of study  
234 region) but are still larger than  $3^\circ$ .

### 235 **3.2 Storm Surge Climate**

236 As noted above, storm surges were defined as events where the water surface elevation exceeded  
237 the 95<sup>th</sup> percentile value,  $\eta^{95}$ . Figure 3 and 4 show plots for each of the sub-regions referenced in  
238 Figure 1. These figures show colour contoured values of  $\Delta C_g E$  (Figure 3) and  $\Delta \theta_m$  (Figure 4),  
239 coastal values of  $\Delta \eta^{95}$  and  $\Delta C_{GA}$ . In contrast to the wave climate, changes in storm surge,  $\Delta \eta^{95}$   
240 are very consistent along the coastline of the study area. Values of  $\Delta \eta^{95}$  are negative along the  
241 entire coastline, decreasing in magnitude from approximately  $-0.3\text{cm/year}$  in the west to  
242  $-0.2\text{cm/year}$  in the east. The fact that the magnitude of storm surges has been decreasing over this  
243 period is consistent with the observations of Liu, et al. (2023) that as Southern Ocean low pressure  
244 systems move south, they increase the mean atmospheric pressure and reduce the pressure gradient  
245 over southern Australia. As surface pressure (and wind) drives storm surge, this results in a  
246 tendency for a reduction in the magnitude of storm surges.

247

### 248 **3.3 Relationship between waves, storm surge and shoreline change**

249 As previously shown at global scale by Luijendijk, et al. (2018) and Ghanavati, et al. (2023),  
250 recession/progradation rates vary in magnitude and sign on relatively small spatial scales. This is  
251 because sediment transport can be both offshore/onshore as well as longshore. In the case of non-  
252 equilibrium longshore transport of sediment, one would expect some beaches to recede whilst  
253 other receive sediment from these beaches and hence prograde. Ghanavati, et al. (2023) speculated  
254 that coastlines which show such non-equilibrium behaviour may be responding to long-term  
255 changes in the environmental forcing provided by trends in waves and storm surge. A causal  
256 relationship is, however, complicated by other variables which may have a larger impact on beach  
257 position. These additional factors include the availability of sediment supplied to beach  
258 compartments from fluvial sources and the impacts of human-induced interventions such as coastal  
259 structures and beach nourishment (Ranasinghe, 2016). Ghanavati, et al. (2023) limited

260 recession/progradation data to values in the range  $\pm 1\text{m/year}$  to confine the datasets to changes  
261 which may be a result of long-term processes rather than fluvial and human-induced influences,  
262 which tend to be much larger in magnitude (Luijendijk, et al., 2018).

263 Therefore, following these precedents, in Figures 3 – 6, the quantity  $\Delta C_{GA}$  has been filtered to retain  
264 only values in the range  $\pm 1\text{m/year}$ . Figure 5 shows values of  $\Delta C_{GA}$  (in the range  $\pm 1\text{m/year}$ ) as a  
265 bar chart along the coastline from  $138\text{E}^\circ$  to  $150\text{E}^\circ$ . Each of the  $2^\circ$  regions shown in Figures 1, 4  
266 and 5 is marked along the longitude axis. As expected, values of  $\Delta C_{GA}$  in Figures 3, 4 and 5 show  
267 both positive (progradation) and negative (recession) values. To quantify recession/progradation,  
268 values of  $\Delta C_{GA}$  in the range  $-0.05\text{m/year}$  to  $-1.00\text{m/year}$  are classified as recession, values in the  
269 range  $+0.05\text{m/year}$  to  $+1.00\text{m/year}$  as progradation and values in the range  $\pm 0.05\text{m/year}$  as  
270 representing stable coastlines. Table 1 shows the percentage of coastal locations classified as  
271 receding, prograding or stable under these criteria. In addition, Figure 6 shows histograms of the  
272 distribution of the magnitudes of the values of  $\Delta C_{GA}$ .

273 Table 1 and Figure 6 show that the sections (c)  $142\text{E}^\circ$ - $144\text{E}^\circ$  and (f)  $148\text{E}^\circ$ - $150\text{E}^\circ$  are  
274 predominately receding. Segment (d)  $144\text{E}^\circ$ - $146\text{E}^\circ$  shows quite large values of both recession and  
275 progradation (see Figure 5) but with more locations prograding than receding. However, this  
276 region is complicated by the presence of Port Phillip Bay. The other segments (a), (b) and (e)  
277 show no clear difference between the percentage of receding and prograding locations.

278 To understand the results shown in Table 1, we consider each of the two degree sections shown in  
279 Figures 3, 4 and 5. In these figures, values of the trend in wave energy flux,  $\Delta C_g E$  (Figure 3) or  
280 wave direction,  $\Delta \theta_m$  (Figure 4) are shown as colour shaded contours over the regions. The trend  
281 in storm surge (always negative) are shown as colour coded squares at  $5\text{km}$  intervals along the  
282 shoreline, at the resolution of the water level model. The satellite-derived values of trend in  
283 shoreline location at each beach location (Bishop-Taylor, et al., 2021) are shown as colour coded  
284 filled circles, at the  $30\text{m}$  along-coast resolution.

285 Figures 3a and 4a show the region from  $138\text{E}^\circ$  to  $140\text{E}^\circ$  (segment (a), Victor Harbour to Cape  
286 Jaffa). This region shows relatively small positive values of  $\Delta C_g E$  (approximately  $0.01\text{kWm}^{-1}$   
287  $/\text{year}$ ) and a small counter-clockwise rotation of the mean wave direct (approximately  
288  $-0.02\text{deg/year}$  or  $0.6^\circ$  over 30 years). In response to these small changes in wave properties there  
289 is no consistent changes in shoreline. In the western regions ( $138.6\text{E}^\circ$ - $139.2\text{E}^\circ$ ) the shoreline is  
290 prograding. However, this may be associated with fluvial sediments, as this region is the ocean  
291 entrance of Lake Alexandrina and the mouth of the Murray River. These results are consistent with  
292 the bar chart of Figure 5 and the results in Table 1 and Figure 6a that there is no clear difference  
293 between recession and progradation for segment (a).



294 Moving east to segment (b), values of  $\Delta C_g E$  increase (Figure 3b) and the region shows small  
295 receding shorelines (139.6E°- 141.0E°). This changes to progradation between 141.0E°-141.2E°,  
296 west of Cape Bridgewater. This behaviour is consistent with sediment being moved along the  
297 shoreline west to east from 139.6E°- 141E° by the increasing wave energy flux and the prevailing  
298 wave direction from the south-west. This sediment transport is interrupted by Cape Bridgewater  
299 resulting in the progradation between 140.8E°-141.2E°. The overall balance between these regions  
300 results in no clear difference between locations receding and prograding in Table 1 and Figure 6b.

301 The strong positive trend in wave energy flux is maintained east of Cape Bridgewater (segment  
302 (c), Figures 3c) with small counter-clockwise rotation of the mean wave direction (Figure 4c).  
303 Along this extended region of the coast to Cape Otway (141.6E°-143.6E°), the coastline shows  
304 small recession (approximately -0.1m/year – 3m over the measurement period of 30 years). East  
305 of Cape Otway, the magnitude of the recession decreases and the shoreline shows little net change  
306 in location. This behaviour is consistent with the reduced impact of south-westerly swell east of  
307 Cape Otway, which provides some shelter from such waves. Table 1 and Figure 6c show that  
308 summed across the full segment (c), a total of 53% of locations are receding and only 27%  
309 prograding.

310 East of Cape Otway, the wave energy flux climate near the coast decreases (Figure 2b), as Cape  
311 Otway provides protection from the south-westerly swell and  $\Delta C_g E$  also decreases as the  
312 protection provided by Tasmania becomes important (Figure 3d). The shoreline trends,  $\Delta C_{GA}$ , are  
313 complicated by the presence of Port Phillip Bay (Figures 3d, 4d). From Cape Otway to Inverloch  
314 (143.6E°- 145.8E°) there is relatively little change in  $\Delta C_{GA}$ . The relatively small region from  
315 Inverloch to Wilson's Promontory (145.8E° - 146.4E°) shows a receding shoreline, previously  
316 noted in studies of the area (Leach, et al., 2023). As a result, there is no clear overall differences  
317 between recession and progradation for this section (Table 1 and Figure 6d). However, if one  
318 considers just the ocean beaches (exclude Port Phillip Bay in Figures 3d and 4d), then there is  
319 small recession along the entire coastline of section (d).

320 East of Wilson's Promontory the coastline is characterized by very long beaches and barrier islands  
321 (Ninety-mile beach). This region from 147E° to 149.6E° (Wilson's Promontory to Cape Howe)  
322 (Figures 3e-f, 4e-f) is characterized by a large counter-clockwise rotation of the mean wave  
323 direction. The region immediately east of Wilson's Promontory (146.5E – 147°E) shows strong  
324 progradation. The remainder of this extended coastline, however, shows consistent recession of  
325 approximately -0.5m/year (15m over the measurement period), particularly for section (f). This  
326 section shows the strongest recession of any extended section, with Table 1 showing 60% of  
327 locations receding and only 30% prograding. As noted above, the dominant swell in this region is  
328 from the south-east and, although the changes in wave energy flux are small, there has been a  
329 significant counter-clockwise rotation of the wave direction over the study period. This results in  
330 the wave direction gradually becoming more shore-parallel. Therefore, the shoreline change noted  
331 above is consistent with an increase in longshore drift (east to west) with sediment being

332 accumulated to the east of Wilson’s Promontory. We should also note that this area east of Wilson  
333 Promontory is one of the few estuarine environments along the entire Victorian coast and hence  
334 some of the observed progradation may be due to fluvial deposits and ebb-tide delta formation  
335 (Konlechner, et al., 2020).

336 The results above use the percentage of coastal locations prograding or receding as the measure of  
337 whether the beach is responding to long term changes in waves and/or storm surge. As such, it  
338 does not consider the magnitudes of the progradation or recession. Figure 6 shows histograms of  
339 the magnitudes of the progradation/recession rates for each coastal sections. The figure confirms  
340 the results above showing sections (c) 142E° – 144E° and (f) 148E° – 150E° are clearly receding  
341 with other sections less clear, as explained for each section above.

342 In the above analysis, we speculate that changes in wave energy flux,  $\Delta C_g E$  and mean wave  
343 direction,  $\Delta \theta$  are the primary drivers of the observed changes in shoreline. The observed data  
344 supports this speculation. The Supplementary Material shows plots similar to Figures 3 and 4 for  
345 changes in the other related quantities: significant wave height,  $\Delta H_s$  (Figures S1 a-c and S1 d-f),  
346 extreme significant wave height,  $\Delta H_s^{95}$  (Figures S2 a-c and S2 d-f), mean wave period,  $\Delta T_m$   
347 (Figures S3 a-c and S3 d-f) and number of extreme wave events,  $\Delta N_{H_s^{95}}$  (Figures S4 a-c and S4 d-  
348 f).

349

#### 350 **4. Discussion, conclusions and future work**

351 Ghanavati, et al. (2023) found that at global scale, they could not distinguish a clear relationship  
352 between modelled (and observed) changes in wave energy flux and storm surge over the last 30  
353 years and changes in shoreline position. The present dataset extends this result by considering the  
354 region of south-east Australia. This region is important in that it is an area with major spatial  
355 variations in wave energy flux climate (mean conditions) and some of the largest coastal trends in  
356 wave energy flux and mean wave direction globally in the last 30 years. In addition, both high  
357 resolution coastal wave and storm surge hindcasts are available, as well as high resolution  
358 observations of shoreline change. As such, this is a unique region to determine if observable  
359 changes in shoreline position are evident as a consequence of long term changes in wave (and/or  
360 storm surge) climate.

361 The results show clear changes in shoreline position, which are consistent with positive trends in  
362 wave energy flux and changes in mean wave direction. In the western regions of the domain the  
363 mean wave direction is from the south-west and there have been positive trends in wave energy  
364 flux,  $\Delta C_g E$  of approximately 14% (6/43kW/m). This appears to have resulted in non-stationary  
365 longshore drift from west to east and shoreline changes of approximately 3m over the 30 year  
366 study period.

367 In the central regions of the study domain both the mean wave energy flux and trends in wave  
368 energy flux decrease, as the island of Tasmania provides protection from the south-westerly swell.  
369 In this region there are no consistent trends in shoreline position with a similar number of coastal  
370 locations receding and prograding. Although ocean beaches do show small recession.

371 To the eastern end of the study domain, the protection provided by Tasmania and the deepwater  
372 counter-clockwise rotation of the mean wave climate means that the wave shadow of Tasmania  
373 results in a relatively large counter-clockwise rotation of the mean wave direction (up to  $6^\circ$  over  
374 the last 30 years). These changes in mean wave direction appear to be driving non-stationary  
375 behaviour of the beach systems in the region with the coastline from  $146^\circ$  to  $149^\circ$  (approximately  
376 300 km) receding by up to 30m over the 30 year study period.

377 The results presented in this analysis are consistent with a study of this same region by Konlechner,  
378 et al. (2020) using lower resolution shoreline change data (Luijendijk, et al., 2018). The shoreline  
379 change “hot-spots” of that study are consistent with the present results. The results of the present  
380 study are also consistent with the global findings of Ghanavati, et al. (2023). Here, we find that  
381 long term changes in wave climate can apparently drive long-term changes in beach location but  
382 that relatively large changes in wave energy flux and/or direction are required to produce  
383 measurable changes in beach position. As noted, the study region has both a very energetic wave  
384 climate and some of the largest trends in this climate of any coastline. **However, even in a region  
385 such as this, where long-term changes in wave energy flux are relatively large, the resulting  
386 changes in beach location are only approximately 1.0 m/year or 30m over the study period.**

387 In the present analysis, we speculate that the observed changes in shoreline position in the western  
388 section of the domain are driven by non-stationary longshore drift from west to east with sediment  
389 transport being intercepted by Cape Bridgewater. Such behaviour is consistent with the observed  
390 increases in wave energy flux and the predominately south-westerly swell. In the eastern sections  
391 of the domain, we speculate that there is sediment transport from the east to west, intercepted by  
392 Wilson’s Promontory. This speculation is consistent with the predominately south-easterly swell  
393 in the region and the observed counter-clockwise change in mean wave direction over the study  
394 period.

395 Although such speculation is consistent with the datasets, other processes may also have an impact  
396 on shoreline change. The most obvious such change is sea level rise, which could be expected to  
397 cause shoreline recession. Observations (Watson, et al., 2015; Nerem, et al., 2018) indicate that in  
398 recent years sea level rise in the Australia region has been approximately 3mm/year. The bed slope  
399 along the south-eastern coast of Australia is on average approximately 1:100 (Athanasίου, et al.,  
400 2019). Therefore, application of Bruun’s rule (Bruun, 1962) would suggest a uniform recession of  
401 approximately 0.3 m/year. Such a value is smaller than, but comparable, to the observed recession  
402 in the western and eastern portions of the study domain. Recession due to sea level rise, however,  
403 would not account for the observed progradation west of Cape Bridgewater or east of Wilson’s  
404 Promontory. In addition, Bishop-Taylor, et al. (2021) indicate that over their full dataset for

405 Australia, approximately the same number of beaches are receding (11.1%) as prograding (11.0%).  
406 Table 1 indicates that for the present study region this is also the case. Sea level rise would be  
407 expected to result in a net recession of beaches. In contrast non-equilibrium longshore drift driven  
408 by changes in wave climate will cause some beaches to recede whilst other prograde.

409 Therefore, we conclude that the present results are more consist with the impacts of changes in  
410 wave climate rather than sea level rise.

411 Although the present study is regional, it has global implications for the magnitude of changes in  
412 shoreline response which may result in other regions of the world under future projections of  
413 changes in wave climate. The present study clearly shows that impacts of changing wave climate  
414 will have strong regional characteristics and that it is important to consider the unique nature of  
415 each region in determining potential impacts. The response to individual coastal compartments  
416 will differ in terms of the magnitude of the response and even the sign (recession verses  
417 progradation).

418 As noted, the present analysis provides the first evidence of a causal relationship between long-  
419 term climate trends in waves and shoreline change. It does, however, have a number of limitations  
420 which should be addressed in future research if a comprehensive understanding of the impacts  
421 future projected changes in wave climate may have on our coastlines. These future studies could  
422 include:

- 423 • Detailed sediment transport modelling to assess whether the observed changes in wave  
424 energy flux and wave direction would be expected to result in non-stationary longshore  
425 drift of the magnitude observed in the recorded shoreline position.
- 426
- 427 • The extraction of shoreline position from relatively low-resolution satellite images is  
428 computationally challenging. The Bishop-Taylor, et al. (2021) dataset represents a  
429 significant advance in resoltion and accuracy. Further developments in the use of Artificial  
430 Intelligence approaches to determining shoreline postion are expected to further reduce  
431 errors in such data.
- 432
- 433 • The present analysis is limited to south-east Australia as there were opportunistic high-  
434 resolution datasets of long-term changes in waves, storm-surge and shoreline position  
435 available. Dedicated projects modelling specific areas for the purpose of better determining  
436 the relationships between changes in these quantities would better quantify the likely  
437 impacts of future changes on vulnerable shoreline.

438  
439

#### 440 **Code/Data availability**

441 All data used in the paper and codes for the analysis are available from the authors upon request.

442

### 443 **Competing Interests**

444 The authors declare no competing interests.

445

### 446 **Author Contributions**

447 MG: Data curation, Investigation, Writing – original draft, Writing – review and editing; IY:  
448 Conceptualization, Investigation, Supervision, Writing – original draft, Writing – review and  
449 editing; EK: Writing – review and editing; JL: Writing – review and editing

### 450 **References**

- 451 Androulidakis, Y. S. et al., 2015. Storm surges in the Mediterranean Sea: variability and trends  
452 under future climatic conditions. *Dynamics of Atmospheres and Oceans*, Volume 71, pp. 56-82.
- 453 Athanasiou, P. et al., 2019. Global distribution of nearshore slopes with implications for coastal  
454 retreat. *Earth System Science Data*, Volume doi.org/10.5194/essd-2019-71.
- 455 Aydoğan, B. & Ayat, B., 2018. Spatial variability of long-term trends of significant wave heights  
456 in the Black Sea. *Applied Ocean Research*, Volume 79, pp. 20-35.
- 457 Barnard, P. et al., 2015. Coastal vulnerability across the Pacific dominated by El Niño/Southern  
458 Oscillation. *Nature Geosciences*, Volume 8, p. 801–807.
- 459 Bishop-Taylor, R., Nanson, R., Sagar, S. & Lymburner, L., 2021. Mapping Australia's dynamic  
460 coastline at mean sea level using three decades of Landsat imagery. *Remote Sens. Environ.*,  
461 Volume 267, p. 112734.
- 462 Bruun, P., 1962. Sea-Level Rise as a Cause of Shore Erosion. *Proc. American Society of Civil*  
463 *Engineers*.
- 464 Cao, Y., Dong, C., Young, I. & Yang, Y., 2021. Global wave height slowdown trend during a  
465 recent global warming slowdown. *Remote Sensing*, Volume 13, p. 4096.
- 466 Cid, A. et al., 2016. Long-term changes in the frequency, intensity and duration of extreme storm  
467 surge events in southern Europe.. *Climate Dynamics*, 46(5), p. 1503–1516.
- 468 Colberg, F., McInnes, K., O'Grady, J. & Hoeke, R., 2018. CSIRO Australia Coastal Sealevel  
469 Simulations. v1. CSIRO. Data Collection. p. <https://doi.org/10.4225/08/5a7280a3a0d2a>.
- 470 Egbert, G. D. & Erofeeva, S. Y., 2002. Efficient inverse modeling of barotropic ocean tides. *J.*  
471 *Atmos. and Ocean. Tech.*, Volume 19, p. 183–204.
- 472 Erikson, L. et al., 2022. Global ocean wave fields show consistent regional trends between 1980  
473 and 2014 in a multi-product ensemble. *Comms. Earth & Env.*, Volume 3, p. 320.

474 Feng, J. et al., 2018. Storm surge variation along the coast of the Bohai Sea. *Scientific Reports*,  
475 8(1), pp. 1-10.

476 Ghanavati, M. et al., 2023. An assessment of whether long-term global changes in waves and  
477 storm surges have impacted global coastlines. *Scientific Reports*, Volume 13, p. 11549.

478 Harley, M. D. et al., 2017. Extreme coastal erosion enhanced by anomalous extratropical storm  
479 wave direction. *Sci. Rep.*, Volume 7, p. 6033.

480 Harley, M., Turner, I., Short, A. & Ranasinghe, R., 2011. A re-evaluation of coastal embayment  
481 rotation: The dominance of cross-shore versus alongshore sediment transport processes,  
482 Collaroy-Narrabeen Beach, southeast Australia. *Jnl. Geophys. Res. (Earth Surface)*, Volume  
483 116.

484 Hemer, M., 2010. Historical trends in Southern Ocean storminess: Long-term variability of  
485 extreme wave heights at Cape Sorell, Tasmania. *Geophys. Res. Lett.*, Volume 37, p. L18601.

486 Hemer, M. et al., 2013. Projected changes in wave climate from a multi-model ensemble. *Nature*  
487 *Clim. Change*, Volume 3, pp. 471-476.

488 Hersbach, H. et al., 2020. The ERA5 global reanalysis. *Q. J. R. Meteorol. Soc.*, Volume 146, pp.  
489 1999-2049..

490 Hinkel, J. et al., 2013. A global analysis of erosion of sandy beaches and sea-level rise: An  
491 application of DIVA. *Global and Planetary Change*, Volume 111, pp. 150-158.

492 Hochet, A. et al., 2021. Sea state decadal variability in the North Atlantic: a review. *Climate*,  
493 Volume 9, p. 173.

494 Kim, D. Y. et al., 2017. Sea Level Rise and Storm Surge around the Southeastern Coast of  
495 Korea.. *Journal of Coastal Research*, 79(10079), pp. 239-243.

496 Komar, P., 1998. *Beach Processes and Sedimentation*. 544pp ed. s.l.:Prentice Hall.

497 Konlechner, T. et al., 2020. Mapping spatial variability in shoreline change hotspots from  
498 satellite data; a case study in southeast Australia. *Estuarine, Coastal and Shelf Science*, Volume  
499 246, p. 107018.

500 Leach, C. et al., 2023. Measuring drivers of shoreline and subaerial beach change using limited  
501 datasets in a temperate, wave-dominated sandy system: Inverloch, Australia. *Ocean Coastal*  
502 *Managment*, Volume 240, p. 106641.

503 Liu, J. et al., 2022. The wave climate of Bass Strait and south-east Australia. *Ocean Modelling*,  
504 Volume 172, p. 101980.

505 Liu, J. et al., 2023. A high-resolution wave energy assessment of south-east Australia based on a  
506 40-year hindcast. *Renewable Energy*, Volume 215, p. 118943.

507 Liu, J., Meucci, A. & Young, I., 2022. Projected wave climate of Bass Strait and south-east  
508 Australia by the end of the twenty-first century. *Climate Dynamics*, pp. 10.1007/s00382-022-  
509 06310-4.

510 Liu, J., Meucci, A. & Young, I., 2023. Projected 21st Century Wind-Wave Climate of Bass Strait  
511 and South-East Australia: Comparison of EC-Earth3 and ACCESS-CM2 Climate Model  
512 Forcing. *Jnl. Geophys. Res.*, Volume 128, p. e2022JC018996.

513 Liu, Q., Babanin, A., Rogers, E. & Zieger, S., 2021. Forty years of global wave hindcasts using  
514 the observation-based source terms: validation and geophysical applications. *Journal of*  
515 *Advances in Modeling Earth Systems*, 13(8).

516 Luijendijk, A. et al., 2018. The state of the world's beaches. *Scientific Reports*, Volume 8, pp. 1-  
517 11.

518 Masselink, G. et al., 2016. Extreme wave activity during 2013/2014 winter and morphological  
519 impacts along the Atlantic coast of Europe. *Geophys. Res. Lett.*, Volume 43, p. 2135–2143.

520 Meucci, A., Young, I., Hemer, M. K. E. & Ranasinghe, R., 2020. Projected 21st century changes  
521 in extreme wind-wave events. *Science Advances*, 6(24), p. eaaz7295.

522 Meucci, A. et al., 2023. 140 Years of Global Ocean Wind-Wave Climate Derived from CMIP6  
523 ACCESS-CM2 and EC-Earth3 GCMs: Global Trends, Regional Changes, and Future  
524 Projections. *Jnl. Climate*, Volume 36, pp. 1605-1631.

525 Meucci, A. et al., 2023. Evaluation of spectral wave model physics as applied to a 100-year  
526 Southern Hemisphere extra tropical-cyclone sea state. *J. Geophys. Res. Oceans*, Volume 128, p.  
527 e2022JC018996.

528 Morim, J. et al., 2022. A global ensemble of ocean wave climate statistics from contemporary  
529 wave reanalysis and hindcasts. *Scientific Data*, Volume 9, p. 358.

530 Morim, J. et al., 2023. Understanding uncertainties in contemporary and future extreme wave  
531 events for broad-scale impact and adaptation planning. *Science Advances*, Volume 9, p.  
532 eade3170.

533 Muis, S. et al., 2016. A global reanalysis of storm surges and extreme sea levels. *Nat. Commun.*,  
534 Volume 7, p. 11969.

535 Nerem, R. et al., 2018. Climate-change-driven accelerated sea-level rise detected in the altimeter  
536 era. *Proc. National Academy of Sciences*, Volume 115, p. 2022–2025.

537 Paprotny, D., 2014. Trends in storm surge probability of occurrence along the Polish Baltic Sea  
538 coast.. *arXiv preprint arXiv*.

539 Ranasinghe, R., 2016. Assessing climate change impacts on open sandy coasts: A review. *Earth-*  
540 *Science Reviews*, Volume 160, pp. 320-332.

541 Ranasinghe, R., R., M., A., S. & G., S., 2004. The Southern Oscillation Index, Wave Climate,  
542 and Beach Rotation. *Marine Geology*, pp. 273-287.

543 Ranasinghe, R. et al., 2021. Climate change information for regional impact and for risk  
544 assessment. . In: *Climate Change 2021: The Physical Science Basis. Contribution of Working*  
545 *Group 1 to the Sixth Assessment Report of the Intergovernmental Panel on Climate Change.*  
546 Cambridge: Cambridge University Press, pp. 1767-1926.

547 Reguero, B. G., Losada, I. J. & Méndez., F. J., 2019. A recent increase in global wave power as a  
548 consequence of oceanic warming.. *Nature communications*, pp. 1-14.

549 Saha, S. et al., 2010. The NCEP Climate Forecast System Reanalysis. *B. Am. Meteorol. Soc.*,  
550 Volume 91, p. 1015–1057.

551 Sen, P., 1968. Estimates of the regression coefficient based on Kendals TAU. *Amer. Stats. Assoc.*  
552 *Journal*, pp. 1379-1389.

553 Shchepetkin, A. F. & McWilliams, J. C., 2005. The regional oceanic modeling system (ROMS):  
554 a split-explicit, free-surface, topography-following-coordinate oceanic model. *Ocean Modeling*,  
555 Volume 9, p. 347–404.

556 Takbash, A. & Young, I., 2020. Long-term and seasonal trends in global wave height extremes  
557 derived from ERA-5 reanalysis data. *J. Mar. Sci. & Eng.*, Volume 8, p. 1015.

558 Timmermans, B., Gommenginger, C., Dodet, G. & Bidlot, J.-R., 2020. Global Wave Height  
559 Trends and Variability from New Multimission Satellite Altimeter Products, Reanalyses, and  
560 Wave Buoys. *Geophys. Res. Lett.*, Volume 47, p. e2019GL086880..

561 Vitousek, S. et al., 2023. A model integrating satellite-derived shoreline observations for  
562 predicting fine-scale shoreline response to waves and sea-level rise across large coastal regions.  
563 *Jnl. Geophys. Res. Earth Surface*, p. e2022JF006936.

564 Vos, K., Harley, M., Turner, I. & Splinter, K., 2023. Pacific shoreline erosion and accretion  
565 patterns controlled by El Niño/Southern Oscillation. *Nature Geoscience*, Volume 16, p. 140–146.

566 Vousdoukas, M. et al., 2020. Economic motivation for raising coastal flood defenses in Europe.  
567 *Nature Comms.*, Volume 11, p. 2119.

568 Wang, X. L. & Swail, V. R., 2001. Changes of extreme wave heights in northern hemisphere  
569 oceans and related atmospheric circulation regimes. *J. Clim.*, pp. 2204-2221.

570 Wang, X. L. et al., 2009. Detection of external influence on trends of atmospheric storminess and  
571 northern oceans wave heights.. *Clim. Dyn.* , pp. 189-203.

572 Watson, C. et al., 2015. Unabated global mean sea-level rise over the satellite altimeter era.  
573 *Nature Climate Change*, Volume 5, p. 565–568.

574 Young, I. & Ribal, A., 2019. Multi-platform evaluation of global trends in wind speed and wave  
575 height. *Science*, Volume 364, pp. 548-552.

576 Young, I. & Ribal, A., 2022. Can multi-mission altimeter datasets accurately measure long-term  
577 trends in wave height. *Rem. Sens.*, Volume 14, p. 974.



578 Young, I., Zieger, S. & Babanin, A., 2011. Global trends in wind speed and wave height.  
579 *Science*, Volume 332, pp. 451-455.

580 Zheng, C. W. & Li, C. Y., 2017. Analysis of temporal and spatial characteristics of waves in the  
581 Indian Ocean based on ERA-40 wave reanalysis,. *Applied Ocean Research*, Volume 63, pp. 217-  
582 228.

583

584

585

586

## 587 **Tables and Figures**

588

<b>Coastal Segment</b>	<b>Recession (-0.05 to -1m/yr )</b>	<b>Progradation (+0.05 to +1m/yr)</b>	<b>Stable (-0.05 to +0.05m/yr)</b>
(a) 138°-140°	40%	45%	15%
(b) 140°-142°	40%	46%	14%
(c) 142°-144°	53%	27%	20%
(d) 144°-146°	37%	49%	14%
(e) 146°-148°	40%	50%	10%
(f) 148°-150°	60%	30%	10%

589

590 Table 1: Percentage of coastal locations, as defined by the Bishop-Taylor, et al. (2021) dataset  
591 receding (-0.05 to -1.00m/year), prograding (+0.05 to +1.00m/year) or stable ( $\pm 0.05$ m/year)  
592 over the period 1988 to 2013.

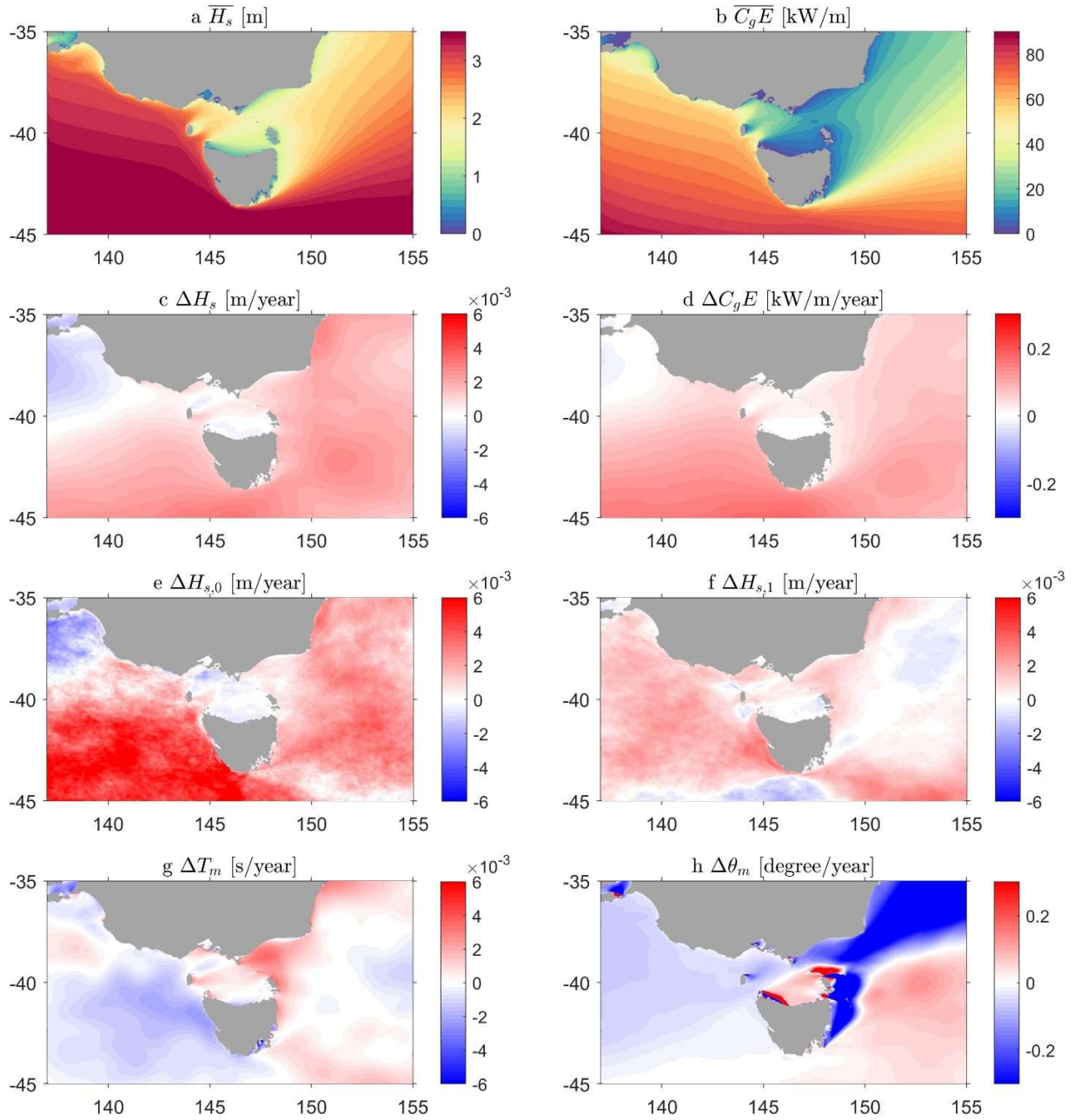
593



594

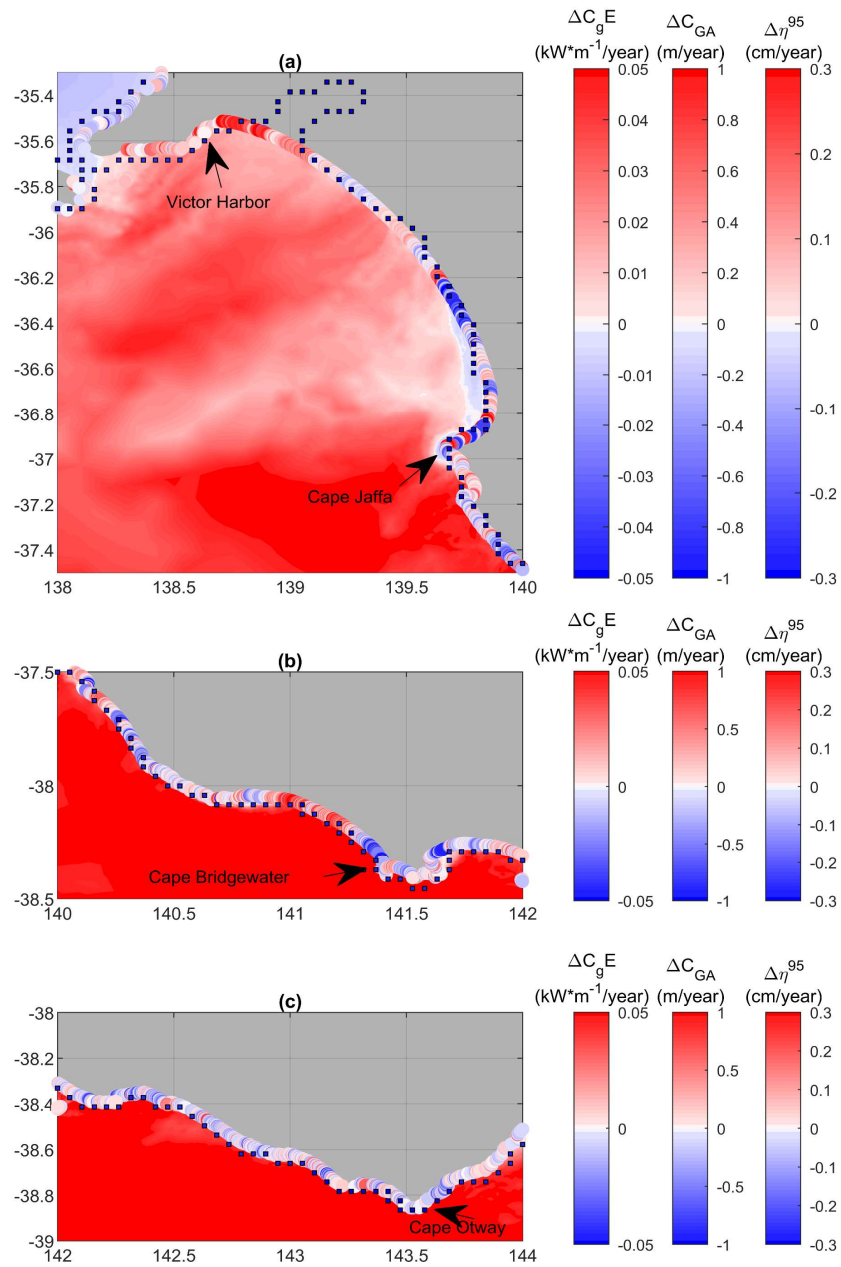
595 Figure 1: The coastal region of south-east Australia comprising the study area. For analysis  
596 purposes the region is divided into six sections: (a) 138°-140°, (b) 140°-142°, (c) 142°-144°, (d)  
597 144°-146°, (e) 146°-148° and (f) 148°-150° from west to east. The island of Tasmania is to the  
598 south of this coastline. (© Google Maps)

599



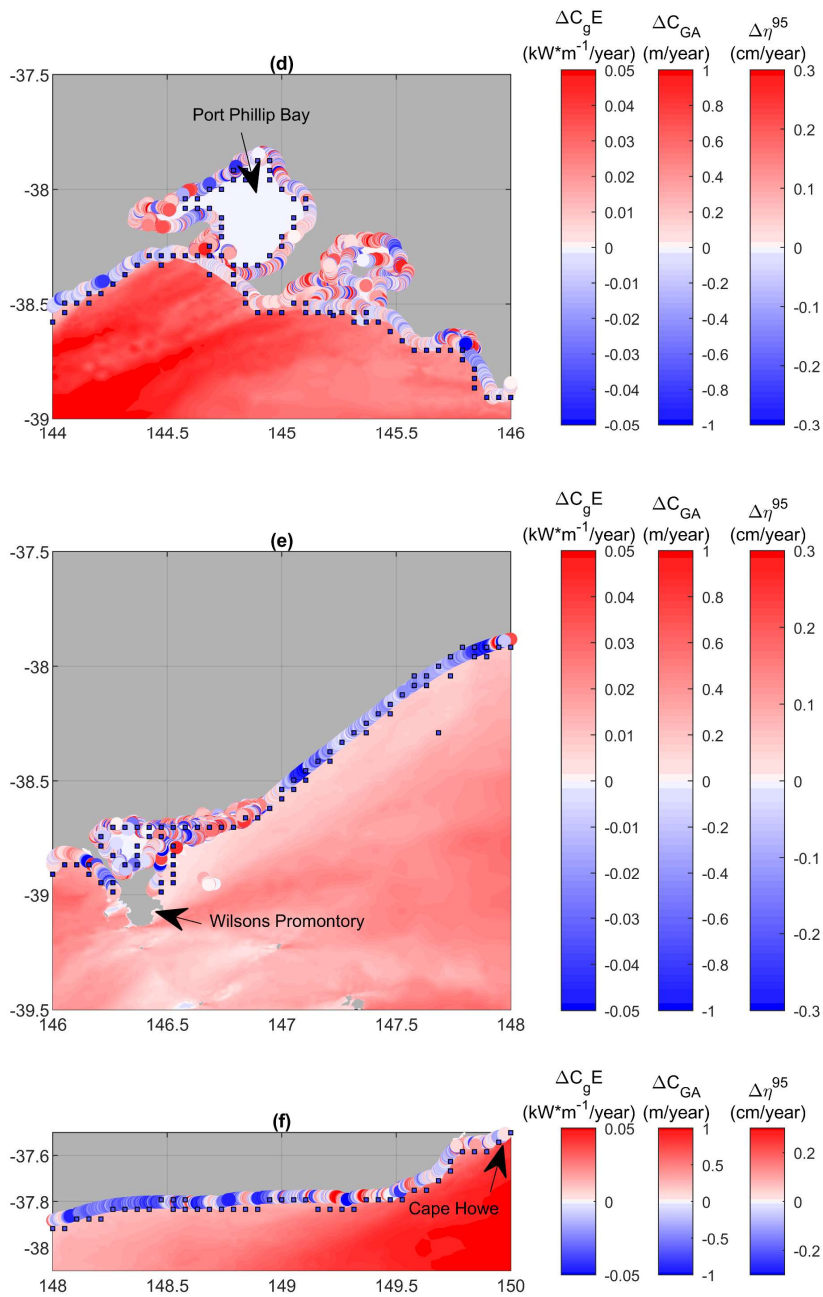
600

601 Figure 2: Wave climate and trends in the study region of south-eastern Australia over the period  
 602 1988 to 2013 as modelled by the Liu, et al. (2022) regional wave model. (a) mean significant  
 603 wave height, (b) mean wave energy flux, (c) trend in significant wave height, (d) trend in wave  
 604 energy flux, (e) trend in wind-wave portion of the spectrum, (f) trend in swell portion of the  
 605 spectrum, (g) trend in mean wave period, (h) trend in mean wave direction.



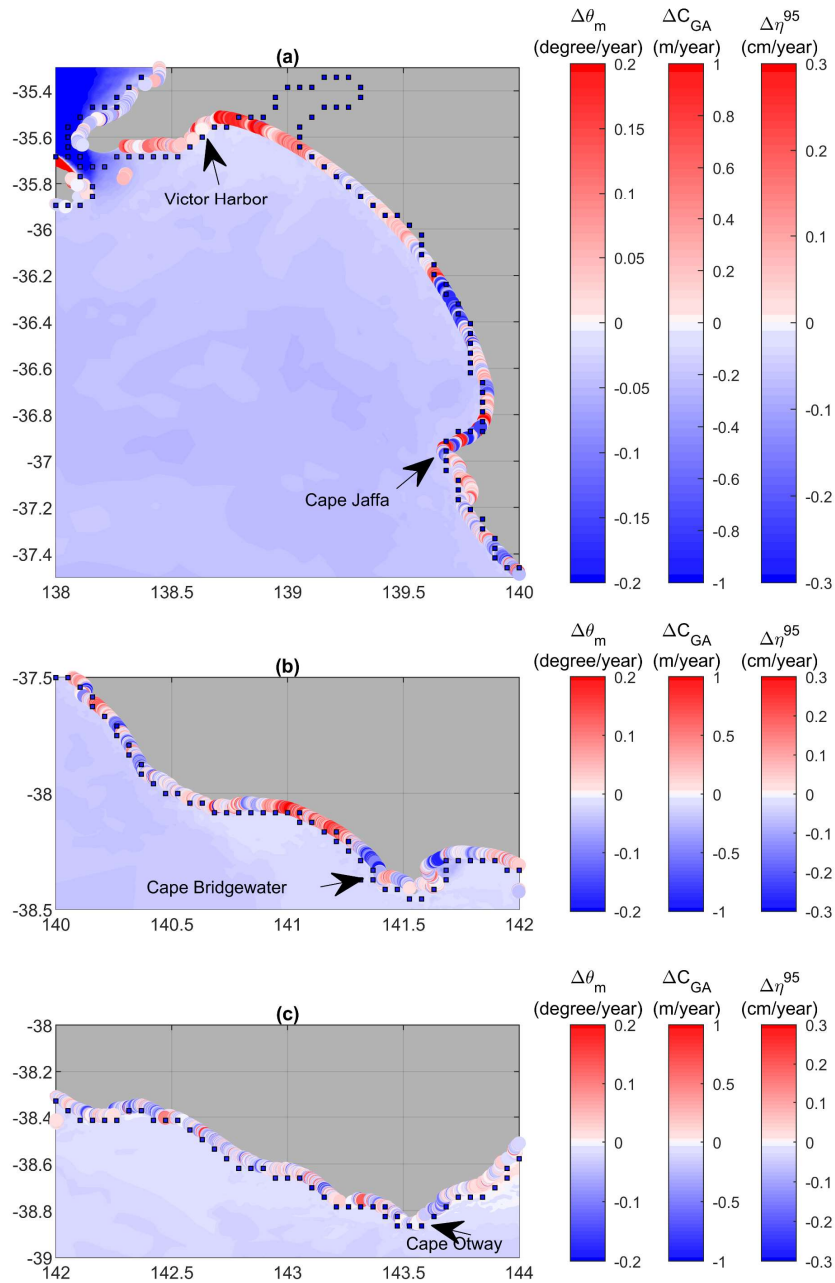
606

607 Figure 3 a-c: Trends in: wave energy flux,  $\Delta C_g E$  shown as colour shaded values over the  
 608 domain, storm surge,  $\Delta \eta^{95}$  shown as colour shaded squares at coastal model locations and  
 609 shoreline progradation/recession,  $\Delta C_{GA}$  shown as colour shaded circles at beach locations.  
 610 Results shown for sections (a) 138E°-140E°, (b) 140E°-142E°, (c) 142E°-144E°.



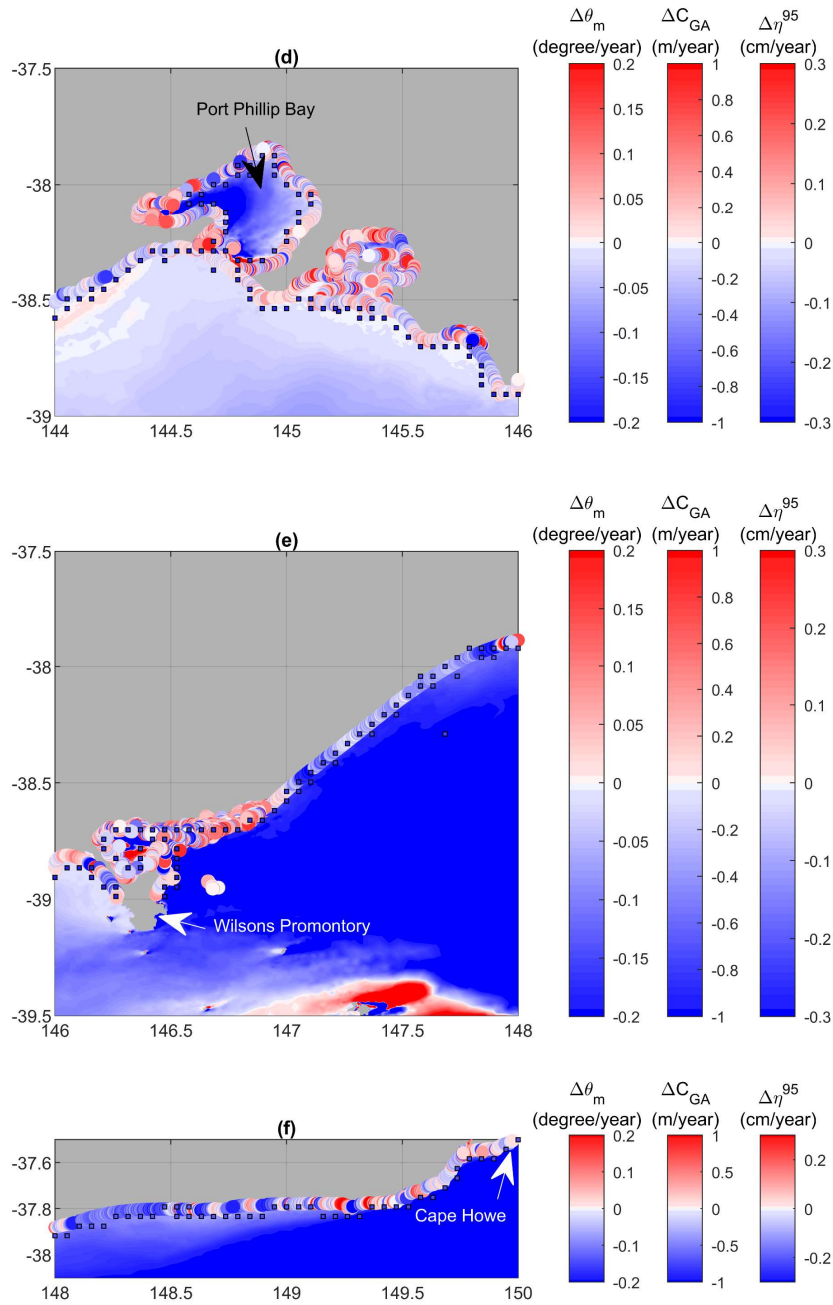
620 Figure 3 d-f: Trends in: wave energy flux,  $\Delta C_g E$  shown as colour shaded values over the  
 621 domain, storm surge,  $\Delta \eta^{95}$  shown as a colour shaded squares at coastal model locations and  
 622 shoreline progradation/recession,  $\Delta C_{GA}$  shown as colour shaded circles at beach locations.  
 623 Results shown for sections (d) 144E°-146E°, (e) 146E°-148E° and (f) 148E°-150E°.

624

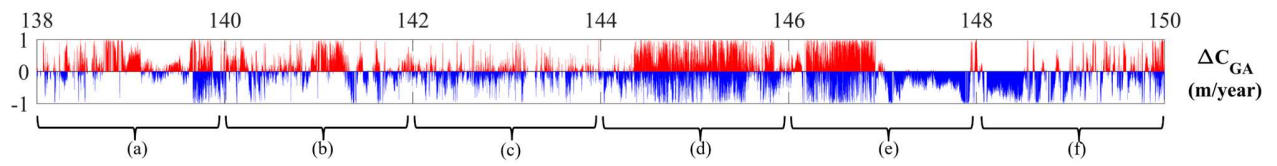


631 Figure 4 a-c: Trends in: mean wave direction,  $\Delta\theta_m$  shown as colour shaded values over the  
 632 domain, storm surge,  $\Delta\eta^{95}$  shown as colour shaded squares at coastal model locations and  
 633 shoreline progradation/recession,  $\Delta C_{GA}$  shown as colour shaded circles at beach locations.  
 634 Results shown for sections (a) 138E°-140E°, (b) 140E°-142E°, (c) 142E°-144E°.





636 Figure 4 d-f: Trends in mean wave direction,  $\Delta\theta_m$  shown as colour shaded values over the  
 637 domain, storm surge,  $\Delta\eta^{95}$  shown as a colour shaded squares at coastal model locations and  
 638 shoreline progradation/recession,  $\Delta C_{GA}$  shown as colour shaded circles at beach locations.  
 639 Results shown for sections (d) 144E°-146E°, (e) 146E°-148E° and (f) 148E°-150E°.

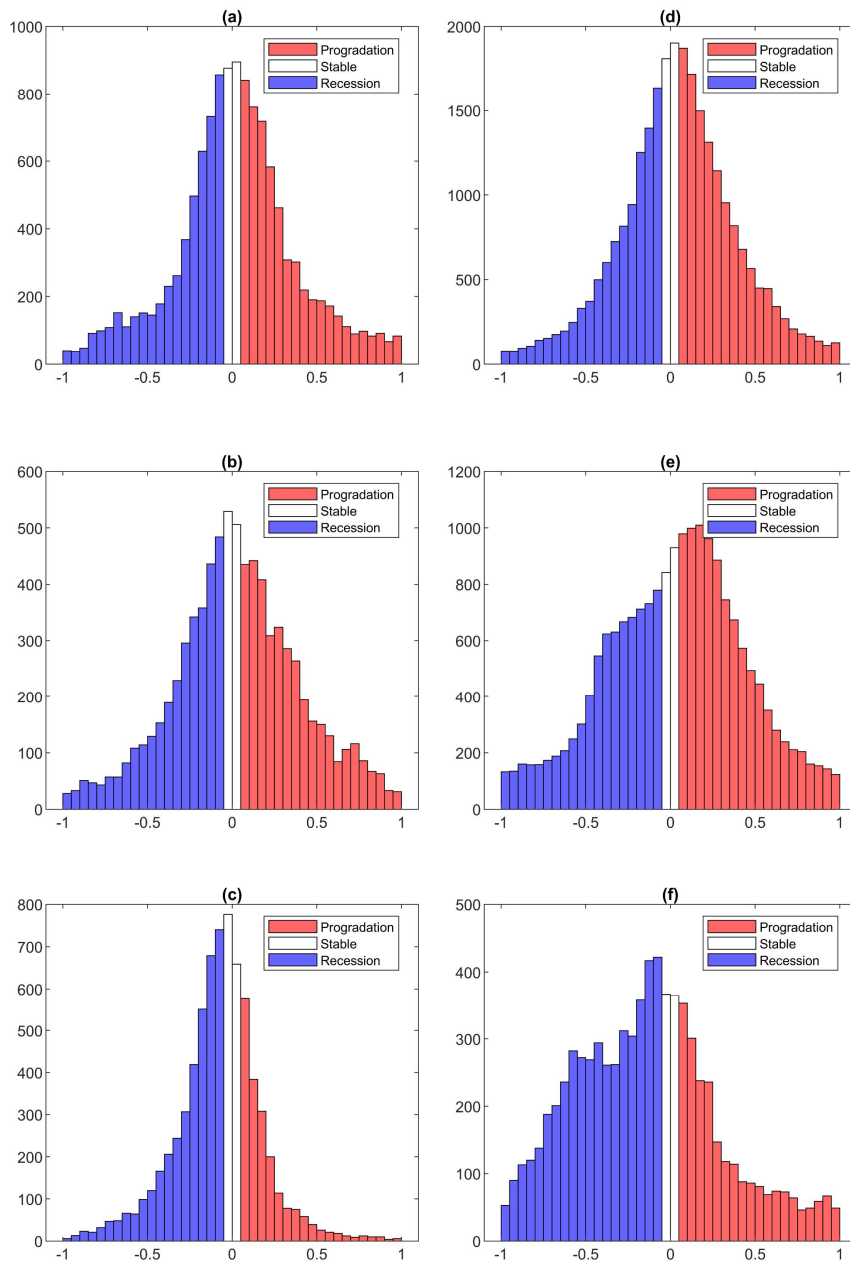


640 Figure 5: Bar chart showing values of progradation (red) and recession (blue),  $\Delta C_{GA}$  at each  
 641 coastal location of the Bishop-Taylor, et al. (2021) dataset. Values are shown as a function of the  
 642 longitude (horizontal axis) and units are m/year. The regions shown in Figure 1 are labelled (a) to  
 643 (f).

644

645





655 Figure 6: Histograms of progradation/recession rates for each of the coastal sections over the  
 656 period 1988 to 2013. (a) 138E°-140E°, (b) 140E°-142E°, (c) 142E°-144E°, (d) 144E°-146E°, (e)  
 657 146E°-148E° and (f) 148E°-150E° from west to east.